Astron. Astrophys. 363, 568–574 (2000)

ASTRONOMY AND ASTROPHYSICS

Van Hoof effect between metallic lines in RR Lyrae

II. Comparison with purely radiative models

M. Chadid[1,2]**, D. Gillet**[3]**, and A.B. Fokin**[4]

[1] European Southern Observatory (ESO), Alonso de Cordova 3107, P.O. 19001, Santiago, Chile (mchadid@eso.org)
[2] Observatoire de la Côte d'Azur, CNRS, Département A. Fresnel, B.P., 4229 Nice, France
[3] Observatoire de Haute-Provence CNRS, 04870 Saint-Michel l'Observatoire, France (gillet@obs-hp.fr)
[4] Institute for Astronomy of the Russia Academy of Sciences, 48 Pjatnitskaja, 109017 Moscow, Russia (fokin@inasan.rssi.ru)

Received 14 April 1999 / Accepted 20 March 2000

Abstract. The differential motion between the photospheric layers of RR Lyrae, where the metallic absorption lines are formed, is calculated with nonlinear nonadiabatic pulsating models recently published by Fokin & Gillet (1997). These atmospheric models are purely radiative and are generated with a Lagrangean code. A comparison between theoretical velocities of two Fe I and Fe II unblended lines shows important differences from the observations around the minimum radius, i. e. when strong shock waves emerge from the photosphere. An analysis of the models indicates that the inadequate modelling of large gradients occurring during this phase interval, is the main disadvantage of this type of models. A complete interpretation of the high quality observations needs the use of more elaborate atmospheric pulsating models.

Key words: hydrodynamics – shock waves – stars: individual: RR Lyr – stars: oscillations – stars: variables: RR Lyr

1. Introduction

Using a nonlocal and time-dependent convective model of RR Lyrae star ($T_{\rm eff} = 6700\,$K, $L = 65\,L_{\odot}$, $M = 0.65\,M_{\odot}$, $X = 0.7$ and $Y = 0.299$), and taking a large enough number of mass zones to model the extended atmosphere, Bono et al. (1994b) predicted the presence of velocity gradients around the phases at minimum radius. In particular, they showed evidence of a phase shift between the base of the atmosphere and the "surface" (layer with the smallest optical depth). They concluded that the base of the photosphere, where weak metal-lines are formed, are affected by substantial variations in physical conditions, and in particular in both opacity and density. These are the physical quantities which cause a velocity gradient and/or which trigger the formation of a shock wave, and in turn the Van Hoof effect.

Recently Chadid & Gillet (1998, hereafter Paper I) detected for the first time the Van Hoof effect between some metallic lines (Fe II-Fe I, Fe II-Ti II, etc.) in the atmosphere of RR Lyrae itself. According to Van Hoof & Struve (1953), this means that the motion of the different photospheric layers is not synchronous. In other words, the pulsation motion of the deep atmosphere already has the form of a running wave. This effect is probably the consequence of the propagation of shock waves in this part of the atmosphere. The existence of prominent shocks at the photospheric level were first detected observationally by Chadid & Gillet (1996a, 1997) and then theoretically confirmed by nonlinear nonadiabatic pulsating models (Fokin & Gillet 1997).

In previous hydrodynamic studies (Hill 1972; Fokin 1992), two main shocks per pulsation period were observed. The first one, called *early shock* and discovered by Hill, was explained by a collision between the free-falling high atmospheric layers and the slower upwarding photospheric layers. It occurs during the bump in the light curve (around phase 0.7). The *main shock* appears near phase 0.9 and is the consequence of the mechanism which is at the origin of the pulsation. A detailed analysis of the physical origin of these shocks has been recently proposed by Fokin & Gillet (1997). In fact, it appears that several shocks are formed during each pulsation period. Their physical origin is of three types.

In classical Cepheids, δ Scuti and β Cephei stars, the Van Hoof effect was detected between Balmer and metallic lines (Van Hoof et al. 1954; Mc Namara et al. 1955; Struve et al. 1955; Yang et al. 1982; Wallerstein et al. 1992; Butler 1993; Mathias & Gillet 1993; Mathias et al. 1997) and between metallic lines themselves (Wallerstein et al. 1992; Mathias & Gillet 1993; Mathias & Aerts 1996). In RR Lyrae stars, Mathias et al. (1995), for the first time, detected the Van Hoof effect between metallic lines and Balmer ones. They interpreted the absence of a Van Hoof effect between metallic lines themselves as the lack of strong shocks within the deep atmosphere. Thus, strong shock waves were thought to be present only in the high atmosphere where the hydrogen line cores are formed, while the metallic ones are created in the photospheric layers.

Today, pulsating atmospheric models of RR Lyrae stars, including shock waves, are starting to be proposed. If the spatial resolution in the atmospheric layers is high enough, the calculation of line profiles and their comparison with high resolution observations would provide the potential to understand the atmospheric motions, as well as to test the accuracy of the models.

Fokin & Gillet (1997) presented two hydrodynamical models of this type, with slightly different parameters in temperature and luminosity. These models are purely radiative and based on a Lagrangean grid, which means that they cannot perfectly describe the hydrogen ionization zone (HIZ) due to a poor space resolution.

Although these models are elaborated enough to confirm the presence of the metallic line doubling in RR Lyrae (Fokin & Gillet 1997), the observational detection of the Van Hoof effect between metallic lines themselves enables us to perform an accurate test of these pulsating models, which we aim to do in this paper.

In Sect. 2 we briefly describe the nonlinear nonadiabatic pulsational models that we use to reproduce the Van Hoof effect observed by Chadid & Gillet (1998). In Sect. 3 the theoretical results concerning the Van Hoof effect between two metallic lines are discussed. The comparison with observations and some concluding remarks are given in Sect. 4.

2. Theoretical models

Pulsating *atmospheric* models for RR Lyrae stars are rare, especially those taking into account convective energy transport. By atmospheric models, we mean those which not only include the large sub-photopheric region containing the main driving and damping zones (H and He ionization zones, Z-peak zone and deeper ones), but also include an extended atmosphere with a sufficient number of mass zones to study the generation and propagation of shock waves. The inclusion of the inner region is necessary to obtain self-consistent pulsating models with realistic amplitudes at the atmospheric level. However, to properly investigate the shock dynamics and its influence on the observed spectral lines, one must include a large number of optically thin atmospheric zones covering the density range from $10^{-8}\,\mathrm{g\,cm^{-3}}$ near the photosphere to at least $10^{-14}\,\mathrm{g\,cm^{-3}}$ at the "surface". We note that such calculations need special numerical techniques to avoid the wave reflection from the surface, as well as much more CPU time. Although in recent years several convective RR Lyrae models have been published (Bono et al. 1997; Feuchtinger 1999), only a few of them have been constructed with extended atmosphere (for instance Davis 1999; Bono et al. 1994b), contrary to radiative models (for instance Fokin 1992; Fokin & Gillet 1997). It is clear that each numerical modelling has its own limits and it is important to check them. The full theoretical description of the Van Hoof effect appears to be one of the best tests for current models to assess their predictive impact.

The two pulsating models, RR41 and RR7b, used in this paper, are described in Fokin (1992) and Fokin & Gillet (1997). We have chosen them after calculating a dozen of RR Lyrae models in order to obtain realistic amplitudes, metal line doubling and other characteristics. Presently, these two atmospheric models are the best ones that we could construct for RR Lyrae. They have been generated with a radiative Lagrangean code, so the spatial resolution in the hydrogen ionization zone (HIZ) is too low to correctly compute the rapid variation of the gas parameters when a shock propagates through this zone. Thus, the intensity and the structure of the shock (described using the von Neuman artificial viscosity), are questionable during this short time. Beyond this short phase, the models are reliable enough.

The parameters of the models are: $T_{\rm eff} = 7175\,\mathrm{K}$, $L = 62\,L_\odot$, $M = 0.578\,M_\odot$, $X = 0.7$ and $Y = 0.299$ for RR41 and $T_{\rm eff} = 6900\,\mathrm{K}$, $L = 62\,L_\odot$, $M = 0.578\,M_\odot$, $X = 0.7$ and $Y = 0.299$ for RR7b. Although RR Lyr is known to pulsate in the fundamental mode, it is located in the Herztsprung-Russell diagram very close to the blue edge of the F-mode instability region and within the first overtone (1H) instability region. Thus, the first overtone is not negligible with respect to the fundamental mode. This explains why we have introduced these two models to take into account the effects of this particular location on the atmospheric dynamics. In particular, our model RR41 is located by 165 K cooler than the fundamental LNA blue edge, and by 565 K cooler that the 1H LNA blue edge. The number of mass layers was 90 and 148, respectively, for RR41 and RR7b. In order to have more spatial resolution, the atmosphere contained 40-50% of the total number of mass zones. The density at the top of the atmosphere is as low as $10^{-14}\,\mathrm{g\,cm^{-3}}$, while the inner boundary was fixed at the temperature of 540,000 K and 770,000 K for RR41 and RR7b, respectively. The total mass of the atmosphere was about 10^{-6} of the stellar mass.

Figs. 1 and 2 show the motion of the mass zones located just below and above the photosphere. This latter is marked by the density "discontinuity", visible approximately between radius 4.84 and 5.55 $\mathrm{R}_\odot$ depending on phase. This discontinuity is caused by the hydrogen ionization zone (HIZ). Note that the mass of each layer is variable, so that the mass fraction between two consecutive layers is $m(i)/m(i+1) = 1.37$ for RR41 and 1.17 for RR7b while the mass of the most outward layer is $10^{-13}\,\mathrm{M_{RR\,Lyr}}$.

From phase 0.4 until the minimum radius at phase 0.97, an accumulation of mass layers appears just above the HIZ. This density bump is the consequence of the large amplitude infalling motion of the atmosphere. As discussed by Fokin & Gillet (1997), several shock waves appear at this phase. In Fig. 2, it is clearly visible that two shocks (noted s4+s3 and s3' by Fokin & Gillet (1997), see their Fig. 4b) merge at the phase 0.73. They are identified by two thick black lines at the outward side of the density bump. Then, the resulting shock (s4+s3+s3') is well observed up to the minimum radius. A consequence of the fast infalling motion on this high density region, is the occurrence of a small "rebound" on its outward part (Fig. 2). A new shock (s1 in Fokin & Gillet 1997) appears near phase 0.85 at the bottom of this region, i.e. just above the HIZ. It merges with s4+s3+s3' at the minimum radius and then, this large amplitude shock quickly propagates outward (Fig. 2).

From Figs. 1 and 2, it appears that the motions of atmospheric layers are not synchronized, contrary to the motion far below the photosphere (not shown here) where the pulsation has the form of a standing wave. In general, the pulsation of the atmosphere (layers above the photosphere) has the form of a running wave. An extreme case of this is the propagation of a shock wave at phase $\varphi = 1$. In this case, the layers just

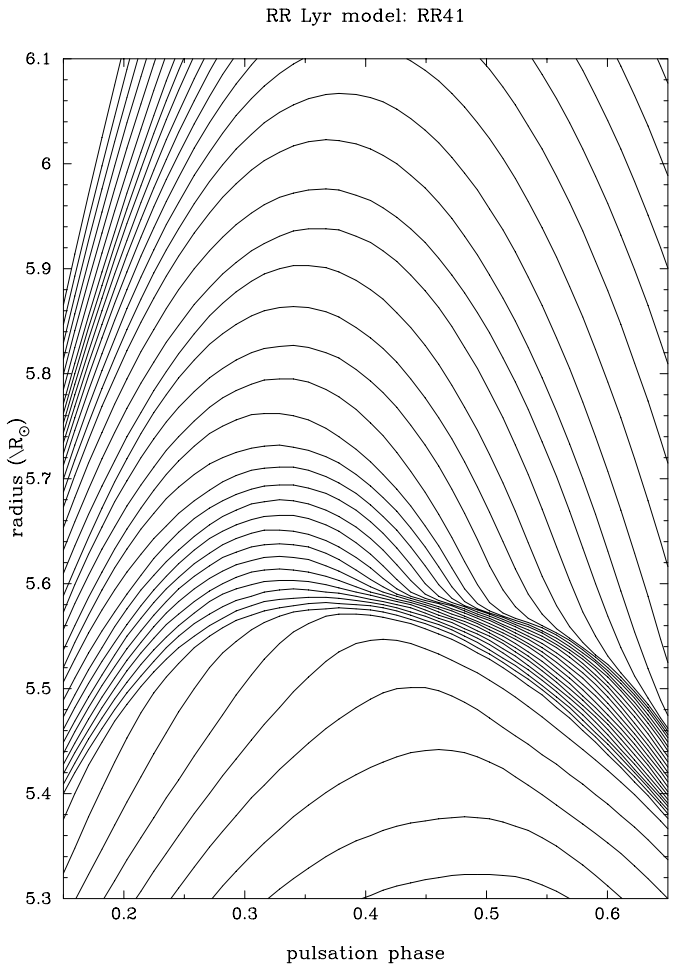

Fig. 1. Motions of different atmospheric layers vs. the pulsation phase for the RR Lyrae model RR41. For this model, there are about 40 mass layers above the photosphere over a total of 90

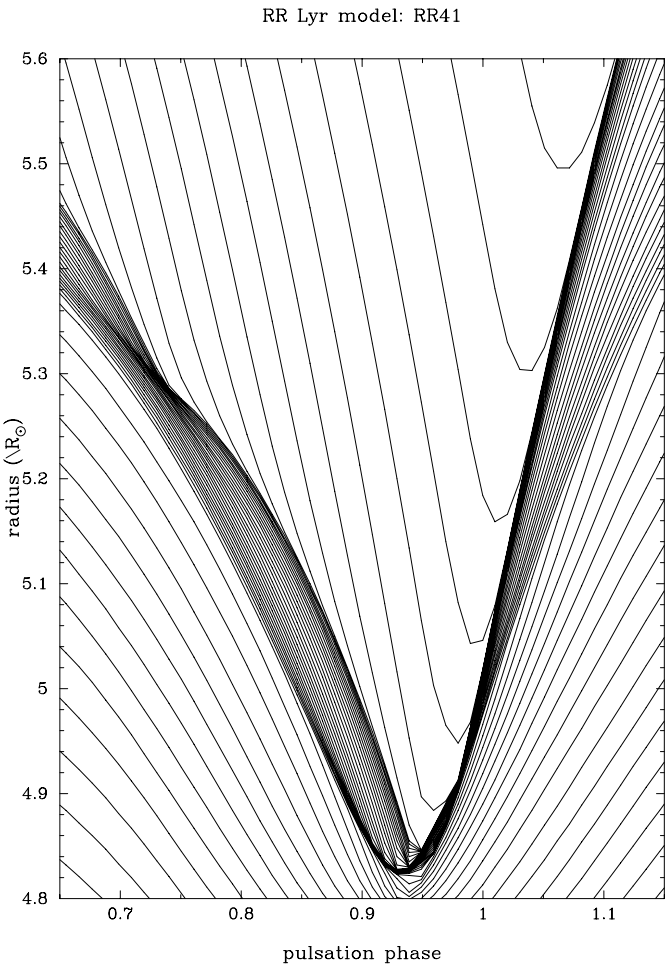

Fig. 2. Same as Fig. 1 except for the following interval phase 0.6-1.2

above the photosphere are propagating outward while the high atmosphere continues its infalling motion. The shock, which reverses the upper layers motion, is located between these two atmospheric regions. The goal of this paper is to check this theoretical result, and in particular to determine if there is a differential motion between deep layers where the metallic absorption lines are formed. For this, we have selected two unblended iron lines, calculated their line profiles vs. pulsation phase and then measured their radial velocities. Of course, because the physical conditions within the atmosphere change during the pulsation, the radial velocity of an absorption line does not always correspond to the same mass layer.

3. Theoretical results

We present first the hydrodynamic model RR41, which reveals the strongest shocks compared to other models. We have chosen two lines: Fe II $\lambda\lambda$ 4923.921 and Fe I $\lambda\lambda$ 4920.509 for which an observational detection of the Van Hoof effect was recently published by Chadid & Gillet (1998). The details of the numerical method of the metallic line calculation are described in Fokin et al. (1996). Theoretical velocities are obtained from a Gaussian fit to whole calculated profiles. Fig. 3 shows the two restframe radial velocity curves while Fig. 4 gives the corresponding velocity-velocity diagram. The phase 0.0 refers to the luminosity maximum and each point in both figures represents an individual line profile.

In Fig. 4, from approximately phase 0.58 to 1.00, the upper loop is described anti-clockwise, in agreement with the observations (Paper I). This means that the Fe II velocity curve is delayed with respect to the Fe I one (see Fig. 3). Contrary to the observational results, the lower loop is also anti-clockwise. Thus, in this model phase 0.96 on the Fe II velocity curve, remains late with respect to that of Fe I during the atmospheric expansion (see Fig. 3). A bump appears between the phases 0.47 and 0.58, and no phase lag is observed from phase 0.3 to 0.47. These two latter features are not present in our observational data (Paper I).

The velocity-velocity diagram of model RR7b (Fig. 7) is similar to that of model RR41, except that the amplitude of the Van Hoof effect around phase 0.95 (upper loop) is extremely weak.

The differential acceleration and velocity curves (Figs. 5 and 8) show two main perturbations. The first one is the effect in-

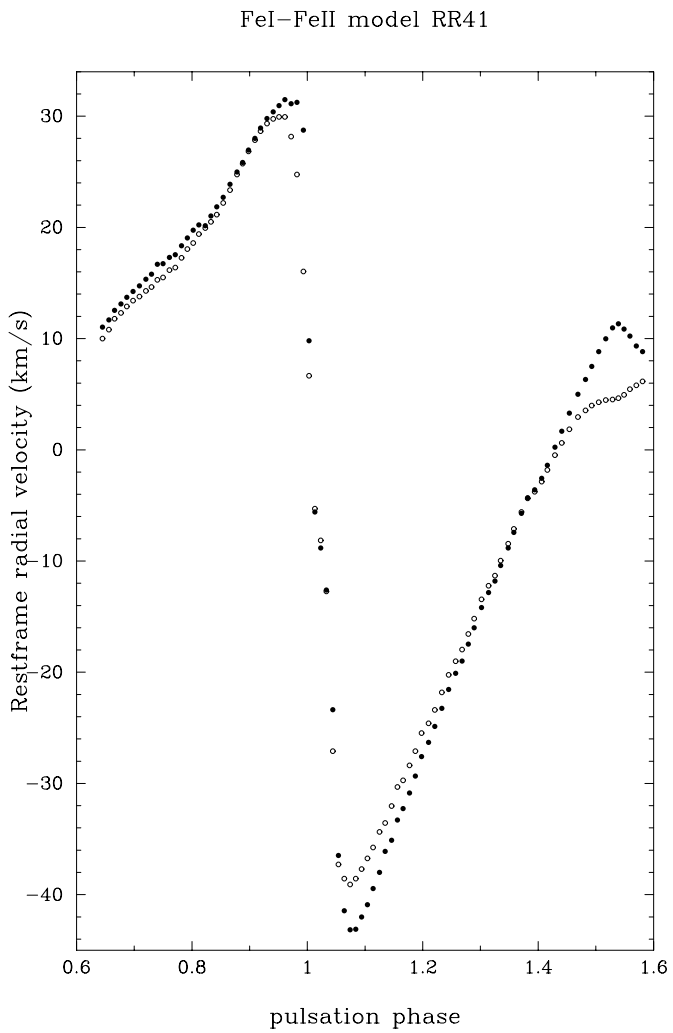

Fig. 3. Theoretical radial velocity curves (model RR41) of Fe II $\lambda\lambda$ 4923.921 (black points) and Fe I $\lambda\lambda$ 4920.509 (white points) deduced from measurements of the calculated Fe II and Fe I line profiles

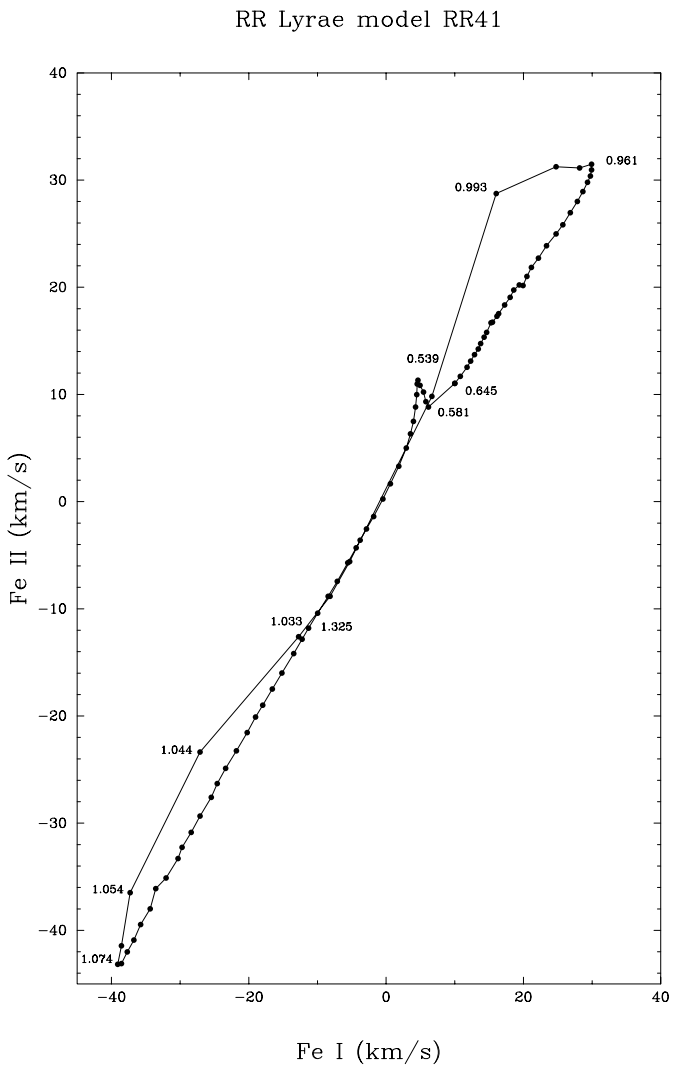

Fig. 4. Theoretical radial velocities of Fe II $\lambda\lambda$ 4923.921 (model RR41) represented versus those of Fe I $\lambda\lambda$ 4920.509. Some pulsational phases are also indicated on the curve

duced by the first weak shock caused by a rebound of the infalling layers just above the HIZ. It is clearly visible around phase 0.55 for RR41 and 0.70 for RR7b. As the pulsation models show, at this phase the Fe I layer is located deeper than the Fe II one. At the same time ΔV increases and when the rebound also affects the Fe I layer, ΔV reaches a maximum, and then comes back to zero. The effect on Δa, is a change in the sign. This inversion of the acceleration indicates that the two metallic layers are clearly separated. During this atmospheric phenomenon, ΔR rapidly increases and becomes positive. Thus, the Fe II layer is now localized below that of Fe I. This inversion is certainly the consequence of the local interplay between the increasing mass density and heating in the line-forming atmospheric layers induced by the rebound shock.

After this first perturbation, the motions of these two layers become well synchronized because the three differential curves are constant for a while. Some weak variations seem present in RR7b but their physical meaning is questionable in the framework of our numerical approach. Note that the Fe II layer remains localized below the Fe I one. Later, at the minimum radius, a rapid inversion of the differential acceleration occurs. It is single for RR7b and double for RR41. For this last model, it corresponds to the passage of two successive strong shock waves across the Fe I and Fe II layers. In Fokin & Gillet (1997) these shocks are denoted as s1 and s2. The passage of s1 produces a larger expansion of the atmosphere than that by s2 because ΔR presents a stronger increase for s1 than for s2. This is consistent with the fact that the amplitudes of s1 and s2 are equal to 125 km/s and 45 km/s, respectively. In RR7b only the shock s1 is visible, because it has an amplitude of 120 km/s while s2 is too weak for an appreciable effect. After the passage of s1 and s2, i.e. during the atmospheric expansion, there is no differential acceleration between the Fe I and Fe II layers. Due to the slow adiabatic cooling of the atmosphere, there is again an inversion of the average line formation height between Fe I and Fe II.

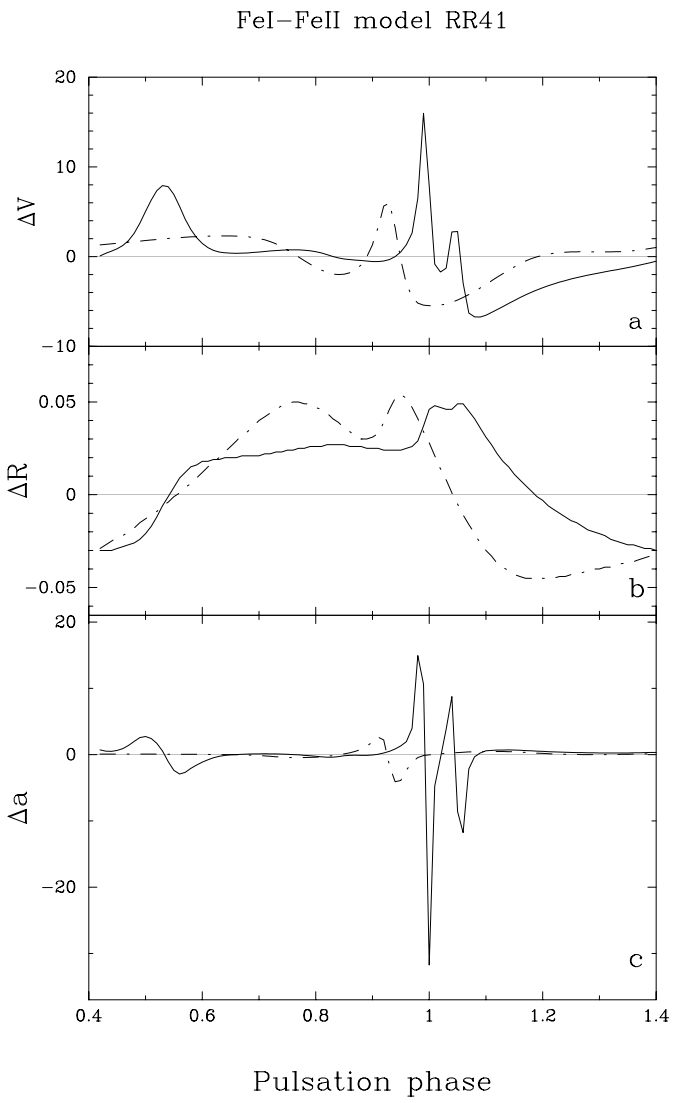

Fig. 5. Theoretical differential velocity ΔV, radius ΔR and acceleration Δa between Fe I $\lambda\lambda$ 4920.509 and Fe II $\lambda\lambda$ 4923.921 lines (model RR41). **a**: $\Delta V = \dot{R}_{\rm Fe\,I} - \dot{R}_{\rm Fe\,II}$ [km.s^{-1}]. **b**: $\Delta R = \int \Delta V {\rm d}t$ [R$_\odot$]. **c**: $\Delta a = \frac{\rm d}{{\rm d}t}(\Delta V)$ [m.s^{-2}]. The dashed-dotted curves show the corresponding observed variations (see Paper I)

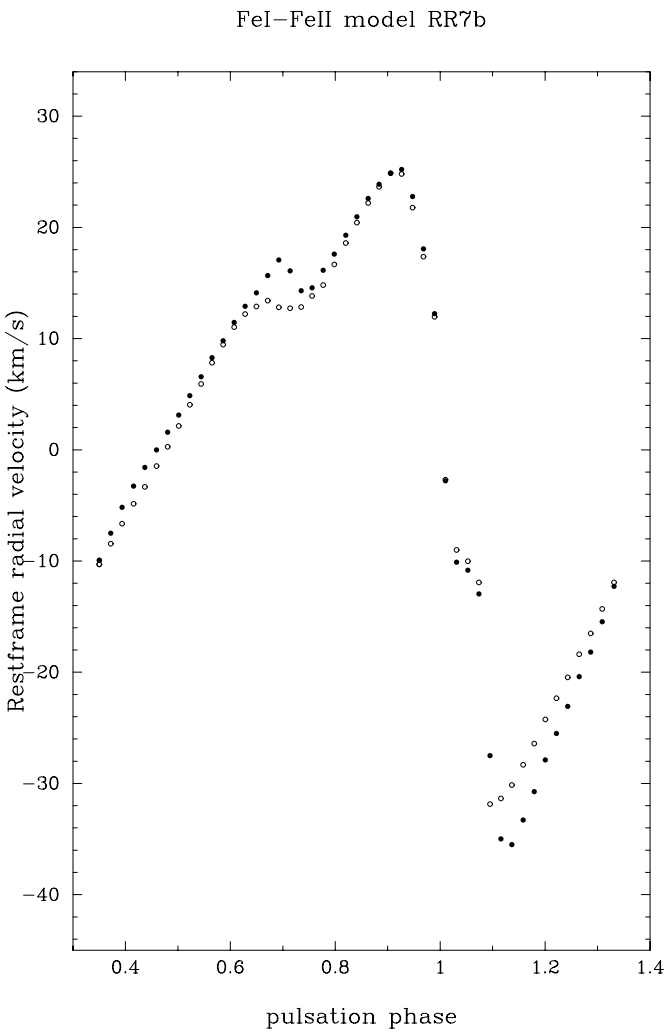

Fig. 6. Theoretical velocity curves (model RR7b) of Fe II $\lambda\lambda$ 4923.921 (black points) and Fe I $\lambda\lambda$ 4920.509 (white points) deduced from measurements of each calculated Fe II and Fe I profiles

4. Comparison with observations and conclusion

The differential velocity ΔV, radius ΔR and acceleration Δa between observed Fe I and Fe II lines are given in Paper I. Contrary to theoretical models, the rebound effect on ΔV and Δa-curves is not detected. Moreover, only one large perturbation is visible at the minimum radius. This means that only one shock has a high enough amplitude to affect the Fe I and Fe II layers, like in RR7b. In this case, only s1 would play a role. Alternatively it may not be possible to distinguish the effect of s1 and s2 due to their small phase separation.

Data plotted in these figures suggest that the shock effects in the models do not occur at the same phase. This shift can be explained by the fact that the effective temperatures of the two adopted models vary from 6900 K for RR7b to 7175 K for RR41. As mentioned in Sect. 2, such temperature differences may lead to different Fourier spectra of the limit cycle pulsation due to the nonlinear influence of the overtones. In turn, this may result in different amplitudes of shocks and alter their dynamics.

The discrepancy between theory and observations suggests that the adopted models do not account for the details of the atmospheric dynamics. Even though a thorough analysis of this mismatch is beyond the aim of this investigation, we briefly mention some plausible reasons. Apart from the uncertainty of the main stellar parameters, the most critical point is the description of the shock waves. Two aspects seem to be important. The first one concerns the numerical modelling of the shock interaction with the HIZ. This problem is typical for all the Lagrangean codes, in which the HIZ is not well spatially resolved.

It is probable that the convection may also alter the result. For example, as shown by the convective models of Bono et al. (1994a), the pulsation amplitudes of these models are smaller that those in the radiative models, which in turn reduce the shock amplitudes. The detailed calculations of the Van Hoof effects

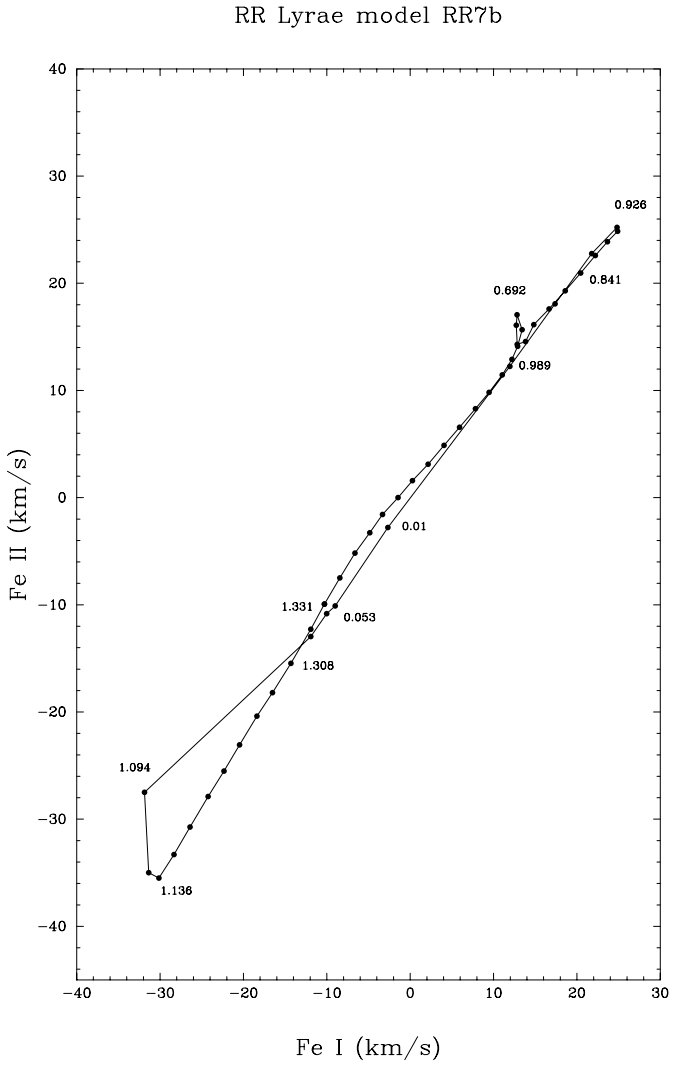

Fig. 7. Theoretical radial velocity of Fe II $\lambda\lambda$ 4923.921 (model RR7b) represented versus that of Fe I $\lambda\lambda$ 4920.509. Also indicated are the pulsational phases for several points

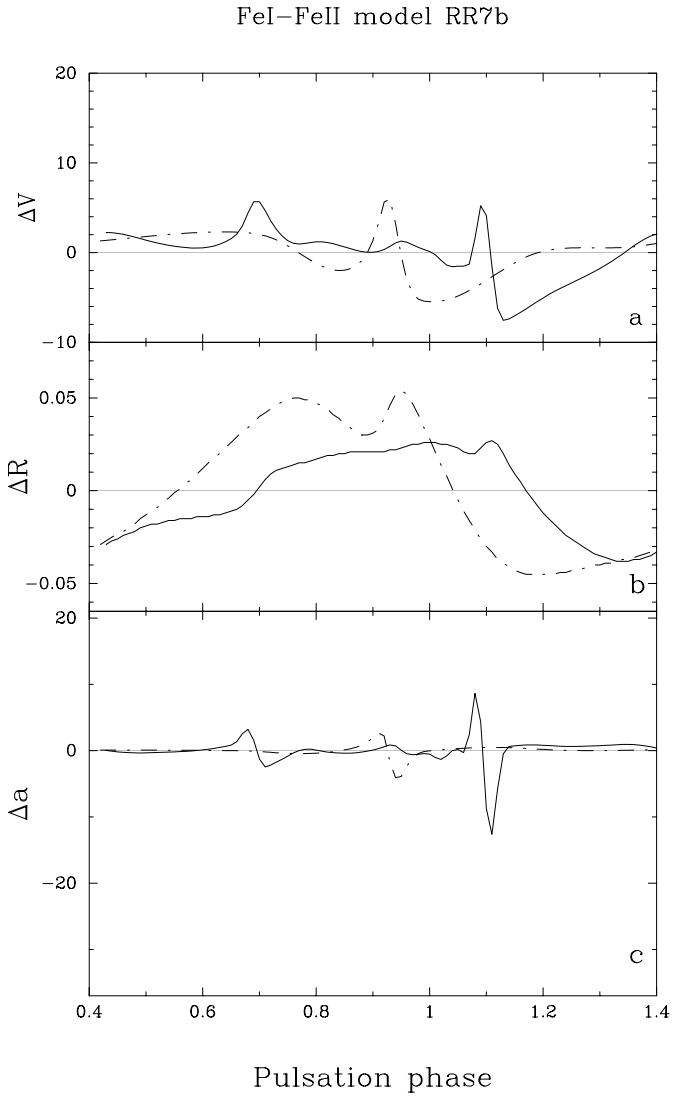

Fig. 8. Theoretical differential velocity ΔV, radius ΔR and acceleration Δa between Fe I $\lambda\lambda$ 4920.509 and Fe II $\lambda\lambda$ 4923.921 lines (model RR7b). **a**: $\Delta V = \dot{R}_{\rm Fe\,I} - \dot{R}_{\rm Fe\,II}$ [km.s^{-1}]. **b**: $\Delta R = \int \Delta V {\rm d}t$ [R$_\odot$]. **c**: $\Delta a = \frac{\rm d}{{\rm d}t}(\Delta V)$ [m.s^{-2}]. The dashed-dotted curves show the corresponding observed variations (see Paper I)

using the convective models are needed to study the effect of convection.

The second aspect concerns the thermal structure of shocks, which is important for the line formation. For instance, the shock heating provokes different variations in the number of absorbers of the Fe I and Fe II lines. Thus, an incorrect calculation of the shock heating/cooling may result in a wrong estimation of the level of formation of each of these lines.

To conclude, this work clearly shows that the study of the Van Hoof effect provides a useful tool to understand the detailed dynamics of atmospheric layers of pulsating stars. It is also a good test for the consistency of the existing (unfortunately not numerous) nonlinear models for pulsating atmospheres. The two models presented, that we have successfully used up to now in less detailed studies of the RR Lyrae, reveal difficulties in reproducing correctly the Van Hoof effect. This means that further improvement of the numerical method, as well as more sophisticated physics, is needed to allow one to interpret the new high-resolution observational data.

Acknowledgements. We would like to express our gratitude to Dr. G. Bono for very constructive comments and suggestions.

References

Bono G., Caputo F., Stellingwerf R.F., 1994a, ApJ 423, 294
Bono G., Caputo F., Stellingwerf R.F., 1994b, ApJ 432, L51
Bono G., Caputo F., Castellani V., Marconi M., 1997, A&AS 121, 327
Butler R.P., 1993, ApJ 415, 323
Chadid M., Gillet D., 1996a, A&A 308, 481
Chadid M., Gillet D., 1996b, A&A 315, 475
Chadid M., Gillet D., 1997, A&A 319, 154

Chadid M., Gillet D., 1998, A&A 335, 255 (Paper I)
Davis C.G., 1999, PASP 111, 196
Feuchtinger M., 1999, A&A 351, 103
Fokin A.B., 1992, MNRAS 256, 26
Fokin A.B., Gillet D., Breitfellner M.G., 1996, A&A 307, 503
Fokin A.B., Gillet D., 1997, A&A 325, 1013
Hill S.J., 1972, ApJ 178, 793
Mathias P., Gillet D., Aerts C., Breitfellner M.G., 1997, A&A 327, 1077
Mathias P., Aerts C., 1996, A&A 312, 905
Mathias P., Gillet D., Fokin A.B., Chadid M., 1995, A&A 298, 843
Mathias P., Gillet D., 1993, A&A 278, 511
Mc Namara D.H., Struve O., Bertiau F.C, 1955, ApJ 121, 326
Struve O., Mc Namara D.H., Zebergs V., 1955, ApJ 122, 122
Van Hoof A., Struve O., 1953, PASP 65, 158
Van Hoof A., De Ridder M., Struve O., 1954, ApJ 120, 179
Wallerstein G., Jacobsen T.S., Cottrell P.L., Clark M., Albrow M., 1992, MNRAS 259, 474
Yang S., Walker G.A.H., Fahlman G.G, Campbell B., 1982, PASP 94, 317